A Parametric Design Method for Engraving Patterns on Thin Shells

Jiangbei Hu, Shengfa Wang, Ying He, Zhongxuan Luo, Na Lei, Ligang Liu

Abstract—Designing diverse, lightweight, and physically viable thin-shell structures is challenging for traditional heuristic methods. We tackle the challenges by developing a novel parametric design framework for engraving regular, irregular, and customized patterns on thin-shell structures. Our method optimizes the pattern parameters (e.g., size and orientation) to ensure structural stiffness under specified material consumption. Our method distinguishes itself from the existing techniques in that it works directly for shapes and patterns represented by functions and can engrave patterns via simple function operations. By completely avoiding the tedious and expensive remeshing step in the traditional FEM methods, our method is more computationally efficient in optimizing mechanical properties. It can substantially enrich the diversity of shell structure design. The quantitative evaluation confirms the convergence of the proposed method. We conduct experiments on regular, irregular, and customized patterns and present 3D printed results to demonstrate the effectiveness of our approach.

Index Terms—Parametric design, pattern engraving, structural optimization, thin shells

✦

1 INTRODUCTION

THIN-shell structures carry loads with their thin and curved shapes, which are particularly elegant and efficient. They can be seen in our living environment in a wide range of dimensions, providing a visual experience of artistic beauty while satisfying mechanical properties [1], [2]. Recently, surface design based on shell structures has received increased interest from both artists and researchers [3], [4], [5]. Among them, engraving is a popular way to design shell structures [6], [7]. After exquisite engraving, the shell structures can have a higher sense of art and lead to medical or lightweight applications [8], [9].

The development of modern computer graphics techniques has led to an increasing diversity of engraving design methods for shell structures, such as those based on texture synthesis [10], tessellation [3], and repetitive patterns [11]. Most existing approaches focus on explicit representation like polygon meshes, which is not conducive to structural analysis and optimal tuning. As a material reduction process, the core problem of engraving design is to maintain the mechanical properties and functions of shell structures in the design process. Due to the high complexity

of topology and geometry of engraved shell structures, it is time-consuming to apply traditional finite element methods(FEM) [12], [13] to mechanical response analysis. Moreover, design, analysis, and optimization are often separated in the existing design techniques, and repetitive remeshing is often required at different stages [14]. Due to a lack of unified representation and effective optimization techniques, engraving design on shell structures is non-trivial.

In this paper, we propose an implicit, parametric method to design lightweight and physically viable thin-shell structures. As shown in Fig. 1, we complete the design by distributing repetitive patterns on the input shell and engraving them. Furthermore, we optimize the attributes of patterns, such as sizes and orientations, to improve the stiffness of the engraved shell structure. We represent the input shell and patterns as implicit functions that can conduct design, analysis, and optimization directly. Since we avoid explicit model generation and remeshing analysis, our method can improve efficiency on the premise of sufficient accuracy compared with the conformal mesh method based on traditional FEM. In our scheme, the patterns can either be hollowed or remain solid, and we refer to the latter as a *dual engraving design*, as shown in Fig. 1(e). Also, because of the inherent implicit property of our method, dual design can be accomplished by simple function modification. We implemented our (dual) engraving design scheme on various shell models and illustrated the effectiveness and efficiency of the method through simulations and comparative experiments.

We summarize our contributions as follows:

- We propose a parametric design method for pattern engraving on thin shell structures based on functions, which can directly represent and design different types of patterns on shells by executing the function operations.
- Based on the implicit representation, we adopt effi-

- *Jiangbei Hu is with DUT-RU International School of Information and Software Engineering and Key Laboratory for Ubiquitous Network and Service Software of Liaoning Province, Dalian University of Technology, and also with the School of Computer Engineering, Nanyang Technological University.*
- *Shengfa Wang* is with DUT-RU International School of Information and Software Engineering, Dalian University of Technology, E-mail: sfwang@dlut.edu.cn*
- *Ying He is with the School of Computer Engineering, Nanyang Technological University.*
- *Zhongxuan Luo is with the School of Software Technology, Dalian University of Technology, and also with Institute of Artificial Intelligence, Guilin University of Electronic Technology.*
- *Na Lei is with DUT-RU International School of Information and Software Engineering, Dalian University of Technology, and also with Beijing Advanced Innovation Center for Imaging Theory and Technology.*
- *Ligang Liu is with the School of Mathematical Sciences, University of Science and Technology of China.*
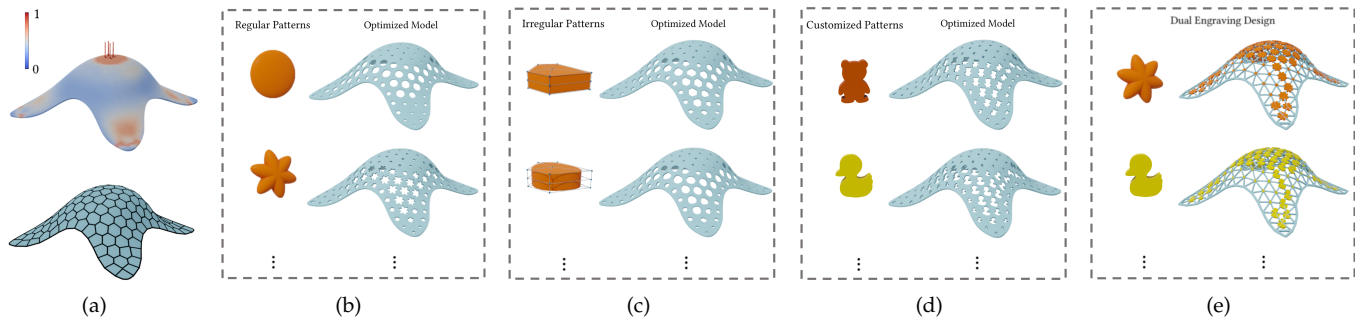
Fig. 1. We develop a parametric design method for engraving patterns on thin-shell structures. It not only enriches design diversity but also enables efficient optimization to improve the stiffness of the structures. (a) Given an input shell model with external loads, we generate the Voronoi tessellation for the medial surface of the shell. (b-d) The optimized shells are (under volume constraint 80%) engraved respectively by regular, irregular, and customized patterns. We use implicit functions to represent all patterns in our scheme. (e) Our method supports dual engraving design (remain patterns as solid) via simple function modifications and also guarantees the mechanical properties using the same optimization frame.

cient modeling and optimization of structural stiffness for engraved thin-shell structures. We solve the optimization problem directly on the implicit representation without remeshing. Computational results show that our method converges quickly.

- Simple function modifications can yield different design solutions. Our framework enriches the diversity of thin-shell structures, which can be applied to physically viable applications, such as medical gears and furniture light-weighting.

2 RELATED WORKS

The development of 3D printing has made it possible to manufacture structures with complex shapes. Meanwhile, many designing and optimization methods based on theories such as computer graphics and structural mechanics have been proposed [15], [16], which can be used to design structures with rich shapes and specific functionalities. The following discusses approaches that are relevant to our work.

2.1 Surface Design on Shells

Designing on thin-shell models has always been a common way for people to create art [17], [18], not only with traditional techniques like paper-cutting and openwork but also many delicate and complex design techniques have appeared recently with the promotion of computer-aided methodology [19], [20].

Texture synthesis. Mature texture synthesis techniques can be used naturally for surface design [21]. Dumas et al. [10] proposed the first method to synthesize textures along a curved surface for digital fabrication. Chen et al. [4] took filigree synthesis design as a packing problem, representing a surface with a set of specified base elements and eventually manufacturing fully connected patterns with good structural performance. In contrast to approaches that generate textures based on basic pattern elements, Zehnder et al. [22] adopted to map planar curves to arbitrary surfaces, which can create structurally-sound curve networks over complex surfaces with a wide variety of aesthetic appeals.

Image carving. Projecting images onto objects and carving them is a traditional decorative technique, but it has been developed thanks to modern technologies. Yang et al. [6] proposed a framework for carving binary images on 3D surface models, which formulates the image carving into image details adaption and structure enhancement problems, and obtains 3D printable and physically-sound designed models. Such techniques can make ordinary objects exquisite and elegant [23].

Tessellations. The compact partition of the space results in a tessellation, a natural and beautiful design shape. Voronoi diagram is one of the potent tools in surface shell design. Pietroni et al. [3] study the relation between optimal anisotropy and density of a grid-shell structure w.r.t. a given stress field and propose a new method to improve the static performance of a grid-shell structure by optimizing its tessellation only. Stadlbauer et al. [7] decomposed the curved surface into a Voronoi-shaped cellular skeletal structure which supports a set of covering shells. Zhang et al. [8] and Rao et al. [9] performed carving designs on personalized orthopedic casts based on Voronoi tessellations, which comfort patients while ensuring lightweight and mechanical properties. Similarly, Ahsan et al. [24] designed honeycomb-like patterns on thin-shell objects. Rib-shell structures based on polygonal meshes are often used in architecture for enhanced stability and ornamentation [25]. Peng et al. [26] present a framework to create mesh patterns that consist of a hybrid of triangles and quads, based on which the artistic design of surface shells is carried out.

Repetitive patterns. Like tiling, designing repetitive patterns to be distributed on curved surfaces is one of the decorative options [19]. The dual shape tiling algorithm developed by Liu et al. [5] yields new manufacturing applications such as decorative window blinds and flexible tiling patterns. Schumacher et al. [11] proposed an automatic optimization algorithm using stencils to design surface shell models, which can optimize stencil parameters with both pattern distribution and stability objectives. Nevertheless, this method simplifies the computational model substantially at the cost of losing accuracy. Distinctively, we design and optimize various patterns engraving directly on function representation. Our engraving framework is different from existing methods in terms of problem formulation and

optimization strategy, which is efficient and significantly enriches the diversity of shell design.

2.2 Structural Optimization

Structural and topology optimization technology has greatly promoted the development of the design and manufacturing field [27].

Topology optimization. Classic topology optimization methods include Homogenization method [28], Solid Isotropic Material with Penalization (SIMP) [29], level-set methods [30], and evolutionary methods [31]. However, these methods usually have high computational costs and a large number of optimization variables. The Moving Morphable Components (MMC) method [32], [33] based on implicit functions expression is able to reduce the computational cost, thereby has attracted more and more attention. Hu et al. [34] also took advantage of the implicit function representation of triply periodic minimal surfaces to optimize the construction of porous structures. Inspired by the implicit optimization method, we propose a parametric design framework for thin-shell structures, which is totally represented, analyzed, and optimized by implicit functions.

Structural design. Topology optimization methods enrich structures' diversity and complexity and simultaneously meet physical properties. There are various structures with different shapes designed based on structural optimization, such as frame structure [35], [36], [37], honeycomb-like structures [38], self-support structures [39], [40], porous structures [41], [42], and so on. The structures are optimized to improve the strength of models [43], the balance [44], or adjust the behaviors [45], [46]. Wu et al. [47] proposed a bone-like porous structure using the SIMP method under local volume constraints. Martínez et al. [48] propose a framework based on topology optimization, which not only enables the structure to possess desirable physical properties but also controls the appearance of the structure according to a user-specified pattern. We also design the appearance and physical properties of shells based on topology optimization, with the difference that we use an implicit approach.

3 OVERVIEW

We propose a parametric design method for (dual) engraving design on thin-shell structures. The pipeline is shown in Fig. 2. First, we construct three types of patterns using function representations, including regular patterns, irregular patterns, and user-specified personalized patterns. These patterns have adjustable properties, such as positions, orientations, and sizes, that can be controlled by parameters (Sec. 4). Then, the patterns are used for engraving on the shell structures. Since we represent the input shells by their signed distance fields, the functional Boolean operation can be performed between the patterns and shell models. Finally, to ensure the soundness of the engraved shell structures, we introduce an optimization model of the structural mechanics problem. With the minimum strain energy as the objective and the given volume as the constraint, the framework can optimize the attribute variables of patterns according to the structural response analysis. The optimized

(dual) engraved shell structures can be simply represented by the zero iso-surfaces of functions (Sec. 5). We have successfully implemented our algorithm on various shell models and have done multiple sets of experiments to validate the effectiveness and robustness of our framework (Sec. 6).

4 PARAMETRIC DESIGN

We use implicit functions in our framework to represent both input models and patterns. As a result, we transfer the complex structure optimization into a controllable parameters design problem, which can be solved in an efficient, robust, and extendable manner.

4.1 Patterns

We propose three types of patterns for engraving design on thin-shell structures, including regular, irregular, and customized ones, all of which can be represented by implicit functions.

4.1.1 Regular Patterns

We first consider rotational symmetric regular patterns and construct them using super-ellipsoid equations,

$$E(\mathbf{r}) = \left(\frac{\hat{x}}{L_1}\right)^p + \left(\frac{\hat{y}}{L_2}\right)^p + \left(\frac{\hat{z}}{L_3}\right)^p - 1, \qquad (1)$$

where $\mathbf{r} = (x, y, z)^\top \in \Omega$ is the design domain in $\mathbb{R}^3$, $\mathbf{c}_0 = (x_0, y_0, z_0)^\top$ is the center coordinates of the super-ellipsoid. Define $\hat{\mathbf{r}} = (\hat{x}, \hat{y}, \hat{z})^\top = \mathbf{R}(\mathbf{r} - \mathbf{c}_0)$, where $\mathbf{R} = \{R_{ij}\}_{3\times3}$ is the rotation matrix to adjust the orientation of the super-ellipsoid. L_1, L_2, and L_3 are the three axes of the super-ellipsoid, respectively, and $p > 0$ is the shape factor which is an even number. The super-ellipsoid approximates a cuboid when p increases.

Multiple super-ellipsoids can constitute rich and complex pattern structures by controlling only a few parameters. We can rotate one super-ellipsoid around its center point in the local coordinate system to get a new pattern, as shown in Fig. 3. Specifically, assuming that a pattern is composed of n super-ellipsoids $\{E_i\}_{i=1}^n$, the rotation angle of the k-th super-ellipsoid should be $\frac{k\pi}{n}$, $k = 1, 2, \cdots, n$. We compute the orientation of super-ellipsoid E_k by the rotation matrix $\Lambda(\frac{k\pi}{n})\mathbf{R}$, where $\Lambda(\theta)$ is the z-axis rotation matrix

$$\Lambda(\theta) = \begin{pmatrix} \cos\theta & \sin\theta & 0 \\ -\sin\theta & \cos\theta & 0 \\ 0 & 0 & 1 \end{pmatrix}. \qquad (2)$$

The regular pattern is the Boolean union of these super-ellipsoids $\{E_i\}_{i=1}^n$, and it can be functionally expressed as

$$P(\mathbf{r}) = \min(E_1, E_2, \cdots, E_n). \qquad (3)$$

In general, a regular pattern described by super-ellipsoids possesses designable parameters $\{\mathbf{c}_0, L_1, L_2, L_3, \mathbf{R}, n, p\}$. One can optimize these parameters according to application requirements to control the artistic and physical properties of patterns engraved shells.

(a) Input Shell   (b) Pattern Design and Layout   (c) Initial Engraving   (d) Optimized Shell   (e) Convergence Curves
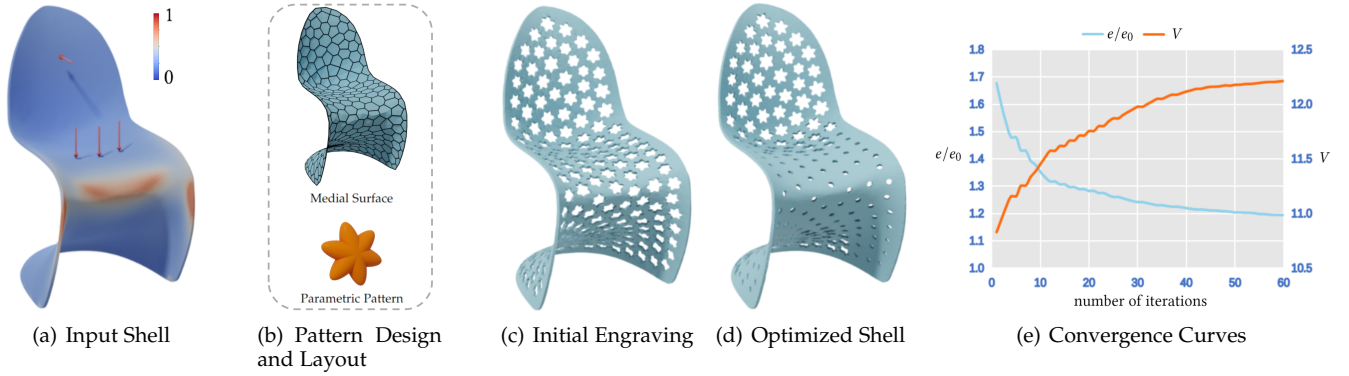
Fig. 2. Illustration of the proposed implicit parametric design and optimization scheme for thin-shell models. (a) Input shell model with external loads and strain energy map. (b) The implicit pattern design and Voronoi tessellation based layout (c) The initial engraved model with regular patterns. (d) The optimized engraved model that obtained under a given volume(75%) with the objective of strain energy minimization. (e) The convergence curves of the relative compliance(e/e_0) and the volume.
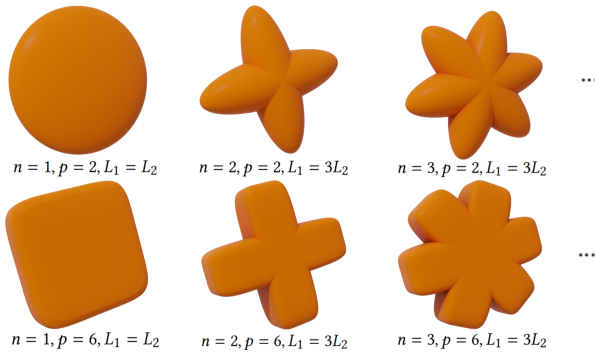

Fig. 3. Regular patterns. The parameters n control the number of super-ellipsoids, $p > 0$ the shapes of super-ellipsoids, L_1, and $L_2 = L_3$ the size of super-ellipsoids.

4.1.2 Irregular Patterns

Irregular patterns are models with free outlines that continuous functions can express. These patterns are designed for engraving based on Voronoi tessellation, which is widely used in various applications. In our method, we utilize B-splines to represent the irregular patterns, and we set the vertices of the Voronoi diagram as the initial control points. As shown in Fig. 4, given a Voronoi cell with vertices $\{\mathbf{p}_i^0\}_{i=1}^m$, centroid $\mathbf{c}_0 = (x_0, y_0, z_0)^\top$, and outward unit normal $\mathbf{n}$, we can set up the new control points of pattern as

$$\mathbf{p}_i = s\mathbf{p}_i^0 + (1-s)\mathbf{c}_0, \tag{4}$$

where $0 < s < 1$ is a shift factor.

In order to construct a closed pattern surface using B-spline, we design the control grid as follows (see Fig. 4(c)),

$$
\begin{aligned}
\mathbf{p}_{i0} &= \mathbf{c}_0 - \frac{h_0}{2}\mathbf{n},\ i = 0,1,\cdots,m, \\
\mathbf{p}_{i1} &= \mathbf{p}_i - \frac{h_0}{2}\mathbf{n},\ i = 1,\cdots,m,\ \mathbf{p}_{01} = \mathbf{p}_{m1}, \\
\mathbf{p}_{i2} &= \mathbf{p}_i,\ i = 1,\cdots,m,\ \mathbf{p}_{02} = \mathbf{p}_{m2}, \\
\mathbf{p}_{i3} &= \mathbf{p}_i + \frac{h_0}{2}\mathbf{n},\ i = 1,\cdots,m,\ \mathbf{p}_{03} = \mathbf{p}_{m3}, \\
\mathbf{p}_{i4} &= \mathbf{c}_0 + \frac{h_0}{2}\mathbf{n},\ i = 0,1,\cdots,m,
\end{aligned}
\tag{5}
$$

where h_0 is the thickness of the input shell structure. Then, we implicitly represent an irregular pattern as

$$P(\mathbf{r}) = ||\mathbf{r} - \mathbf{c}_0|| - d(u, v) = 0, \tag{6}$$

where $d(u, v)$ is a distance function that can be interpolated as

$$d(u, v) = \left\| \sum_{i=0}^{m}\sum_{j=0}^{4} N_{i,\xi}(u)N_{j,\eta}(v)\mathbf{p}_{ij} - \mathbf{c}_0 \right\|, \tag{7}$$

where $\|\cdot\|$ is the Euclidean norm on $\mathbb{R}^3$, $N_{i,\xi}(u)$ and $N_{j,\eta}(v)$ are B-spline basis functions with surface parameters u and v [49]. We set $u \in [-\pi, \pi]$, $v \in [0, \pi]$ and adopt uniform spaced knots. ξ and η are orders of B-spline basis functions. In our experiments, $\eta = 2$ and ξ is used to control the smoothness of irregular pattern. For irregular patterns, the designable variables are $\{\mathbf{c}_0, s, \xi\}$.
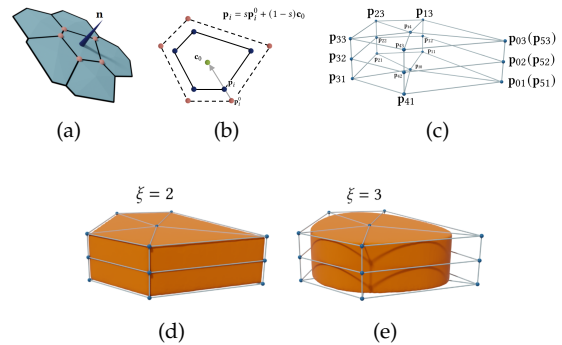

Fig. 4. Irregular patterns. (a) Our method uses a Voronoi cell with normal to determine the shape of an irregular pattern. The user can adjust the pattern size by shifting the control points as shown in (b). We show the control grids in (c), and two examples of irregular patterns with different smoothness parameters ξ in (d) and (e), respectively.

4.1.3 Customized Patterns

Customized Patterns are models with user-customized personalized outlines. A customized pattern should be a sheet flat model whose thickness is related to the thickness of input shell structures. To construct the customized pattern in a standardized way, we calculate the minimum circles that enclose the 2-dimensional outlines of the patterns [50]

and limit the sizes of patterns by the radius of the circles. Taking the center of a minimal circle as the center of the local coordinate system, we can obtain a customized pattern with thickness h_0 by offsetting the plane model along the z-axis. To unify the functional representation, we fit the customized patterns using radial basis functions. Similarly, we apply a scaling factor $\mathbf{s} = (s_x, s_y, s_z)^\top$ and a rotation matrix $\mathbf{R}$ to control the size and orientation of patterns. Finally, we represent the customized pattern as the zero isosurface of the fitted function

$$P(\mathbf{r}) = \sum_{i=1}^{m} \omega_i \varphi(\|\hat{\mathbf{r}} - \mathbf{r}_i\|) + Q(\hat{\mathbf{r}}) = 0, \qquad (8)$$

where $\hat{\mathbf{r}} = \mathbf{s}^\top \mathbf{R}(\mathbf{r} - \mathbf{c}_0)$, $\mathbf{c}_0 = (x_0, y_0, z_0)$ is the center coordinates of the pattern, and $\{\mathbf{r}_i\}_{i=1}^{m}$ are the uniform sampling points in the domain occupied by the pattern ($m = 1000$ by default), $\varphi(t) = t^2 \log(t)$ is the thin-plate spline basic function, $Q(\mathbf{r}) = \omega_{m+1}x + \omega_{m+2}y + \omega_{m+3}z + \omega_{m+4}$, and $\{\omega_i\}_{i=1}^{m+4}$ are fitting coefficients.
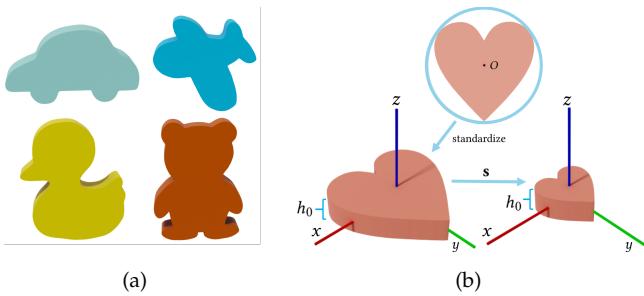

Fig. 5. Customized patterns. (a) User-customized sheet flat structures can construct customized patterns. (b) The standard pattern (left) has the same thickness as the input shell structure. We then can adjust the pattern (right) by scaling the standardized pattern, keeping the thickness unaltered.

As shown in Fig. 5, once a standardized pattern is constructed, we scale the pattern with the unaltered thickness. That is, the scaling factor should satisfy $s_x = s_y$ and $s_z = 1$. Therefore, the variables of the customized patterns that can be designed are $\{\mathbf{c}_0, s_x, \mathbf{R}\}$.

4.2 Engraving

The problem of engraving patterns on shells is the implementation of Boolean operations between the input shells and the patterns. Thanks to the representation based on functions, the complex Boolean operations can be simplified to calculate a minimum of functions.

4.2.1 Pattern Parameters

We characterize a pattern by its position, orientation and size.

Position. It is crucial to distribute the patterns on shell structures. As shown in Fig. 6 (b), we first compute a restricted centroidal Voronoi tessellation on the medial surface using Lloyd method [51]. Then, we place the patterns at the centroids of the Voronoi cells with centers $\{\mathbf{c}_0^i = (x_0^i, y_0^i, z_0^i)\}_{i=1}^{N_p}$, where (x_0^i, y_0^i, z_0^i) is the centroid of the i-th Voronoi cell and N_p is the number of patterns. Voronoi tessellation has been widely used for shell design

and is compatible with the designed irregular pattern. We can apply our framework to optimize the location of the patterns. However, the optimized variables and costs will increase dramatically. Therefore, we exploit the Voronoi diagram to simplify the algorithm's computation. It is desirable to explore a more efficient, optimized way to determine the positions of patterns in the future.

Orientation. The orientation of patterns consists of two steps: set the z-axis directions and the rotation orientations on the xy-plane in the local coordinate systems, respectively. First, we rotate the pattern by the orientation matrix $\mathbf{R}_i^z$ so that the z-axis direction of the local coordinate system is aligned with the normal vector $\{\mathbf{n}_c^i\}_{i=1}^{N_p}$ of the corresponding Voronoi cell on the medial surface. Specially, if $\mathbf{n}_c^i = \mathbf{z}_0$, where $\mathbf{z}_0 = (0, 0, 1)^T$, the orientation matrix $\mathbf{R}_i^z = \mathbf{I}_{3\times3}$; Otherwise, $\mathbf{R}_i^z$ can be calculated as

$$\begin{aligned} \mathbf{n}_z^i &= \mathbf{n}_c^i, \\ \mathbf{n}_x^i &= \frac{\mathbf{n}_x^i \times \mathbf{z}_0}{\|\mathbf{n}_x^i \times \mathbf{z}_0\|}, \\ \mathbf{n}_y^i &= \frac{\mathbf{n}_z^i \times \mathbf{n}_x^i}{\|\mathbf{n}_z^i \times \mathbf{n}_x^i\|}, \\ \mathbf{R}_i^z &= (\mathbf{n}_x^i, \mathbf{n}_y^i, \mathbf{n}_z^i)^T. \end{aligned} \qquad (9)$$

Then, we determine the orientations of patterns on xy-plane in the local coordinate systems by rotating the patterns according to the rotation angles. As a result, the orientation of patterns can be confirmed by a rotation matrix as,

$$\mathbf{R}_i = \Lambda(\alpha_i)\mathbf{R}_i^z, \qquad (10)$$

where $\{\alpha_i\}_{i=1}^{N_p}$ are designable rotation angles that can be optimized. Moreover, our method allows us to determine the rotation angles by generating a directional field [52], as shown in Fig. 6 (c). A regular directional field allows for a more aesthetically pleasing distribution of patterns.

Size. The patterns should be confined inside the corresponding Voronoi cells to avoid intersections. Moreover, the adjacent patterns should not be too close to guarantee printability and usability. That is, we set the maximum dimensional length of the i-th pattern as

$$L_{\max}^i = e_b^i - \epsilon/2, \qquad (11)$$

where e_b^i is the minimum distance between the current center point and the Voronoi cell boundaries and ϵ is the minimum printing accuracy. The minimum dimensional length of the pattern can be specified according to the applications. In our experiments, we set the minimum dimensional length $L_{\min}^i$ of the i-th pattern as half of the thickness of the input shell by default.

4.2.2 Engraving on Shells

To design shell structures implicitly, we represent the input shell models by their signed distance functions $\phi_{\text{shell}}(\mathbf{r})$. The design of engraving on shells is to remove the parts of the shell. Since both the patterns and the input shell are represented by functions, we can transfer the complex Boolean operation into the following simple calculation

$$\Phi^E(\mathbf{r}) = \min(\phi_{\text{shell}}(\mathbf{r}), P_1(\mathbf{r}), P_2(\mathbf{r}), \cdots, P_{N_p}(\mathbf{r})), \quad (12)$$
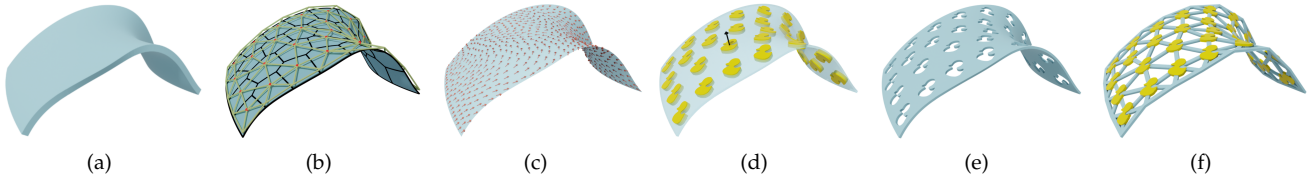
Fig. 6. Algorithmic pipeline. (a) Input shell model. (b) The Voronoi tessellation on the medial surface and its corresponding Delaunay triangles. (c) The specified directional field. (d) Distribution of patterns. (e) and (f) The engraved model and dual engraving design represented using functions, respectively.

which satisfies

$$\Phi(\mathbf{r}) \begin{cases} > 0, & \text{if } \mathbf{r} \text{ is inside the designed model,} \\ = 0, & \text{if } \mathbf{r} \text{ is on the designed model boundary,} \\ < 0, & \text{if } \mathbf{r} \text{ is outside the designed model.} \end{cases}$$
(13)

The engraved shell structure is the zero isosurface of function $\Phi(\mathbf{r})$, as shown in Fig. 6 (e).

4.2.3 Dual Engraving Design

Alternatively, the part of patterns intersecting the shell can be retained solid rather than hollowed, which we call dual engraving design. In our study, we implement dual engraving through simple function modification. All the reserved solid parts can be expressed as

$$\phi_{\text{retain}} = \max(\tilde{P}_1(\mathbf{r}), \tilde{P}_2(\mathbf{r}), \cdots, \tilde{P}_{N_p}(\mathbf{r})),$$
$$\tilde{P}_i(\mathbf{r}) = \min(\phi_{\text{shell}}(\mathbf{r}), -P_i(\mathbf{r})), \ i = 1, 2, \cdots, N_p.$$
(14)

To connect the individual patterns, we construct a set of truss structures using the edges of the dual Delaunay triangles of the Voronoi tessellation, as shown in Fig. 6 (b). For opened surface, we also need to add edges to connect the boundary points of Delaunay triangles and the boundary points of Voronoi tessellation. Assuming the Delaunay triangles have edges set $\{e_i\}_{i=1}^{N_e}$, we use the super-ellipsoid equations described in Eq. (1) to construct the truss structures

$$\phi_{\text{truss}} = \max(\tilde{E}_1(\mathbf{r}), \tilde{E}_2(\mathbf{r}), \cdots, \tilde{E}_{N_e}(\mathbf{r})),$$
$$\tilde{E}_i(\mathbf{r}) = \min(\phi_{\text{shell}}, E_i(\mathbf{r})), \ i = 1, 2, \cdots, N_e,$$
(15)

where $\{E_i(\mathbf{r})\}_{i=1}^{N_e}$ is a series of super-ellipsoids, and we set the midpoint of each edge as the corresponding super-ellipsoid's center. The direction of the edge determine the rotation matrix $\mathbf{R} = \{R_{ij}\}_{3\times3}$. L_2 is set to half of the edge length, L_1 and L_3 are released to be optimized to adjust the thickness of the truss structures locally. For constructing trusses, we set $p = 8$. In our experiments, L_1 and L_3 are assigned according to the strain energy distribution of the input shell under the external loads. Finally, the dual engraving can be implicitly represented as

$$\Phi^{DE}(\mathbf{r}) = \max(\phi_{\text{retain}}, \phi_{\text{truss}}).$$
(16)

Similarly, we extract the zero isosurface of the function $\Phi^{DE}(\mathbf{r})$ to get the dual engraving shell structure, as shown in Fig. 6 (f).

5 FORMULATION AND OPTIMIZATION

The design method described above can be applied to various physically viable applications, such as furniture design, medical gear optimization, and lightweight composite structures. Based on the implicit representation, we adapt an automatic and efficient optimization directly on functions. We formulate the modeling and optimization for mechanical application.

5.1 Problem Formulation

Structure compliance is a physical quantity that measures the global structural stiffness, often used in classical topology and structure optimization [29], [30]. Introducing the shape description function $\Phi(\mathbf{r})$, we define the structure compliance as

$$I = \int_{\Omega_S} H(\Phi(\mathbf{r}))\mathbf{f} \cdot \mathbf{u} \, dV + \int_{\Gamma_t} \mathbf{t} \cdot \mathbf{u} \, dS,$$
(17)

where Ω_S is the region occupied by the input shell model S, $\mathbf{f}$ is the body force, $\mathbf{t}$ is the surface traction defined on the Neumann boundary Γ_t, $\mathbf{u}$ is the displacement, and $H(x)$ is the regularized Heaviside function [32]

$$H(x) = \begin{cases} 1, & \text{if } x > \eta, \\ \frac{3(1-\alpha)}{4}(\frac{x}{\eta} - \frac{x^3}{3\eta^3}) + \frac{(1+\alpha)}{2}, & \text{if } -\eta \le x \le \eta, \\ \alpha, & \text{if } x < -\eta, \end{cases}$$
(18)

where η and α are the parameters that control the magnitude of regularization and the non-singularity of the global stiffness matrix, respectively. In our experiments, we set $\alpha = 0.001$ and η to one-fiftieth of the maximum size of the input shell model. We take the minimization of the structure compliance (Eq. (17)) as the objective of optimization under the volume constraint $\overline{V}$,

$$V = \int_{\Omega_S} H(\Phi(\mathbf{r})) \, dV \le \overline{V},$$
(19)

Considering the static mechanical problem, given the fixed boundary constraint like

$$\mathbf{u} = \overline{\mathbf{u}}, \, on \, \Gamma_u,$$
(20)

we write the equilibrium equation in its weak, variational form as

$$\int_{\Omega_S} H(\Phi(\mathbf{r}))\mathbb{E} : \varepsilon(\mathbf{u}) : \varepsilon(\mathbf{v}) dV$$
$$= \int_{\Omega_S} H(\Phi(\mathbf{r}))\mathbf{f} \cdot \mathbf{v} \, dV + \int_{\Gamma_t} \mathbf{t} \cdot \mathbf{v} \, dS, \forall \mathbf{v} \in \mathcal{U}_{ad},$$
(21)

where $\overline{\mathbf{u}}$ is the specified displacement on the Dirichlet boundary Γ_u, $\mathbf{v}$ is the test functions defined on Ω_S, $\mathcal{U}_{ad} = \{\mathbf{v}|\mathbf{v} \in W^1(\Omega_S), \mathbf{v} = \mathbf{0}\ on\ \Gamma_u\}$, W^1 is a one-order Sobolev space, ε is the second order linear strain tensor, $\mathbb{E}$ is an elasticity tensor defined by the Young's Modulus and the Poisson ratio.

5.2 Computation and Optimization

5.2.1 Discrete Computation.

The shell structure after engraving has complex topology and geometry, which will lead to high computational complexity. Remeshing (tetrahedral or hexahedral) is needed in each iteration in traditional finite element based optimization, which is very time-consuming. Thanks to the fact that the proposed shell structures with engraved patterns are represented by functions, remeshing is not needed to represent the models. Only uniform finite elements that served as the integration domain are required to construct once, and then we execute the integration and derivative calculations directly on the functions.

Moreover, we also utilize a super element strategy [53], [54] to accelerate the calculation. As shown in Fig. 7, we divide the design domain Ω_S uniformly into coarse, regular hexahedral elements called super elements, which are used to interpolate the displacement field. Then, we divide each super element evenly into smaller regular hexahedral elements called background elements, which are used to precisely depict the geometry with high resolution. The direct calculation using functions and the integration domain with a super element strategy prompt our optimization much more efficiently than the traditional finite element based methods (FEM), especially for complex engraved shell structures.
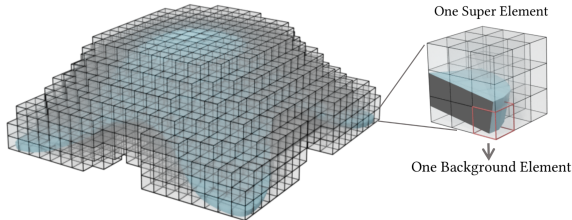

Fig. 7. Super element strategy. We use super and background elements to interpolate the displacement field and precisely describe the geometry, respectively.

5.2.2 Optimization.

With the above discretization scheme, we reformulate the optimization problem Eq. (17-21) as

$$\min_{\Theta}\ \mathbf{F}^T\mathbf{U}, \tag{22}$$

$$\text{s.t.:}\ \mathbf{K}\mathbf{U} = \mathbf{F}, \tag{23}$$

$$V = \frac{1}{8}\sum_{j=1}^{N_b}\sum_{l=1}^{8} H(\Phi_l^j)v_b \le \overline{V}, \tag{24}$$

where Θ is the set of parameters to be optimized. In our experiments, we use different parameters to determine the attributes of different patterns, such as $\Theta =$

$\{\{L_1^i\}_{i=1}^{N_p}, \{\alpha_i\}_{i=1}^{N_p}\}$ for regular patterns, $\Theta = \{s_i\}_{i=1}^{N_p}$ for irregular patterns and $\Theta = \{\{s_x^i\}_{i=1}^{N_p}, \{\alpha_i\}_{i=1}^{N_p}\}$ for customized patterns. $\mathbf{U}$ is the vector of displacements, $\mathbf{F}$ is the nodal force vector, N_b is the number of background elements, and $\mathbf{K}$ is the stiffness matrix with the $i\text{-}th$ element

$$\mathbf{K}^i = \sum_{j=1}^{N_b}\frac{1}{8}\sum_{l=1}^{8}(H(\Phi_l^{ij}))\mathbf{K}^0, \tag{25}$$

where Φ_l^{ij} is the value of $\Phi(\mathbf{r})$ at the $l\text{-}th$ node point of the $j\text{-}th$ background element in the $i\text{-}th$ super element, $\mathbf{K}^0$ is a constant matrix in each background element,

$$\mathbf{K}^0 = \varepsilon_0\mathbf{B}(\mathbf{r}_{ij})^T\mathbf{D}^0\mathbf{B}(\mathbf{r}_{ij})v_b, \tag{26}$$

where ε_0 is the original elasticity modulus, $\mathbf{B}$ is the strain matrix, $\mathbf{r}_{ij}$ is the coordinate vector of the integration point associated with the $j\text{-}th$ background element in the $i\text{-}th$ super element, and $\mathbf{D}^0$ corresponds to the constitutive matrix of the solid material, and v_b is the volume of one background element. Since we only need to update the coefficient $\frac{1}{8}\sum_{l=1}^{8} H(\Phi_l^{ij})$ in each iteration, the stiffness matrix $\mathbf{K}$ can be assembled efficiently during the response analysis.

We solve the optimization problem Eq. (22) using GCMMA [55], [56], which is a gradient-based algorithm for topology optimization. We compute the gradient of the objective function and constraint directly on the implicit representation as

$$\frac{\partial I}{\partial\Theta} = -\sum_{k=1}^{N_s}\mathbf{U}_k^T\left[\frac{1}{8}\sum_{j=1}^{N_b}\left(\sum_{l=1}^{8}\frac{\partial H(\Phi_l^{kj})}{\partial\Theta}\right)\mathbf{K}^0\right]\mathbf{U}_k, \tag{27}$$

$$\frac{\partial V}{\partial\Theta} = \frac{1}{8}\sum_{j=1}^{N_b}\sum_{l=1}^{8}\frac{\partial H(\Phi_l^j)}{\partial\Theta}v_b, \tag{28}$$

where Θ is the set of parameters to be optimized, N_s and N_b are the numbers of super elements and background elements, respectively. All our experiments achieved convergent solutions within 120 iterations.

6 EXPERIMENTAL RESULTS AND DISCUSSIONS

In this section, we conduct numerous experiments to verify the effectiveness, robustness, and applicability of our method.

6.1 Validity

To demonstrate the validity of the analysis, we compare the strain energy maps obtained by the FEM software ANSYS[1] and our super elements strategy under the same loading conditions. We use the default SOLID186 element in ANSYS, a 20-node solid element exhibiting quadratic displacement behavior, to mesh the engraved shell structures. Given that we formulate the structure optimization problem as compliance minimization, we compare the compliance values of structures under different experimental configurations. We take the normalized compliance e/e_0 as the evaluation metric for structural stiffness, like Wu et al. [47] did, where
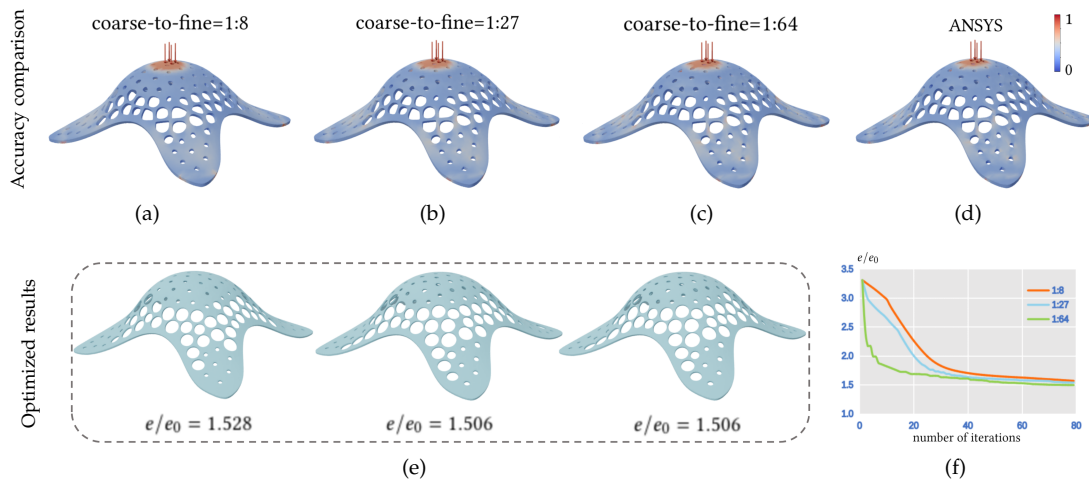
1. https://www.ansys.com/

Fig. 8. Analysis validity. (a)-(c) Strain energy maps obtained by our method with varying coarse-to-fine ratios (super elements/ background elements). (d) Strain energy map calculated by ANSYS. (e) The corresponding optimized results under the same volume constraint (66%), where e_0 and e are the total energy of the original shell structure and the optimized structure, respectively. (f) The corresponding convergence curves.
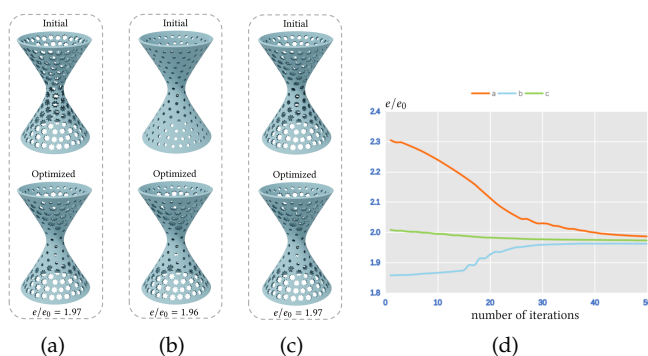

Fig. 9. Robustness. (a)-(c) The optimized models with different initialization (pattern size). (d) The corresponding convergence plots.

e_0 is the compliance of original shell structure. As Fig. 8 shows, the energy distributions of our results with different coarse-to-fine ratios (super elements/ background elements) are all comparable to the result of ANSYS on the same models. It demonstrate the validity and accuracy of the super element approach for the compliance minimization problem. The finer the elements, the more accurate the results will be, but it will increase the computation time simultaneously. In Fig. 8 (e), we show the corresponding optimized results under the same volume constraint (66%) with different coarse-to-fine ratios ($1:8$, $1:27$, and $1:64$). In the trade-off between accuracy and efficiency, we choose the coarse-to-fine ratio $1:27$ by default in our experiments.

6.2 Effectiveness and comparison

The proposed method can achieve convergence efficiently even with different initial values. As shown in Fig. 9, the shell models with different initial patterns converge to similar results under the same loading conditions and constraints. To verify the robustness of the proposed framework, we test more complex shell models with different types of patterns, as illustrated in Fig. 10. All the experiments achieved convergence within 120 iterations.

To verify the effectiveness, we demonstrate the effectiveness and efficiency comparison between ANSYS (standard commercial software using traditional FEM) and our method in Table 1. Compared with the results of ANSYS, although there are numerical differences in the energy calculation results, we can see from Fig. 8 that the relative energy distribution is comparable. It indicates that our scheme can accurately find the collapse-prone areas of the structure and optimize them. Meanwhile, our optimization time is much less than ANSYS because we omit the time-consuming re-meshing in each iteration.

We also compare the proposed method with the method based on discrete triangle elements similar to [11], as shown in Fig. 11. They propose a parameterized algorithm for stenciling using an example-based texture synthesis method, which is an explicit method implemented on the discrete representation. The strain energy for each triangular cell in their method is constant, which significantly loses accuracy. Unlike this discrete method, our method is implemented directly on implicit functions. Benefiting from this, our approach can be easily controlled by function parameters, is more diverse, and can be extended to different optimization problems. For example, we can also optimize a dual problem to enrich the diversity of thin-shell structures. Our method generates optimized structures with greater structural stiffness (smaller compliance ratio e/e_0) than the comparison results under the same volume constraint (75%). Because the method in [11] computes structural deformation with constant strain triangle elements, it suffers accuracy loss, especially for complex geometry shells. Moreover, our method has better controllability and extensibility because it is executed based on the function representation. As shown in Fig. 10, we extend the implicit framework to dual engraving design, which enriches the diversity of shell structures.

6.3 3D Printing and Testing

All the optimized engraved models can be well manufactured by 3D printers, as shown in Fig. 12. To prove the

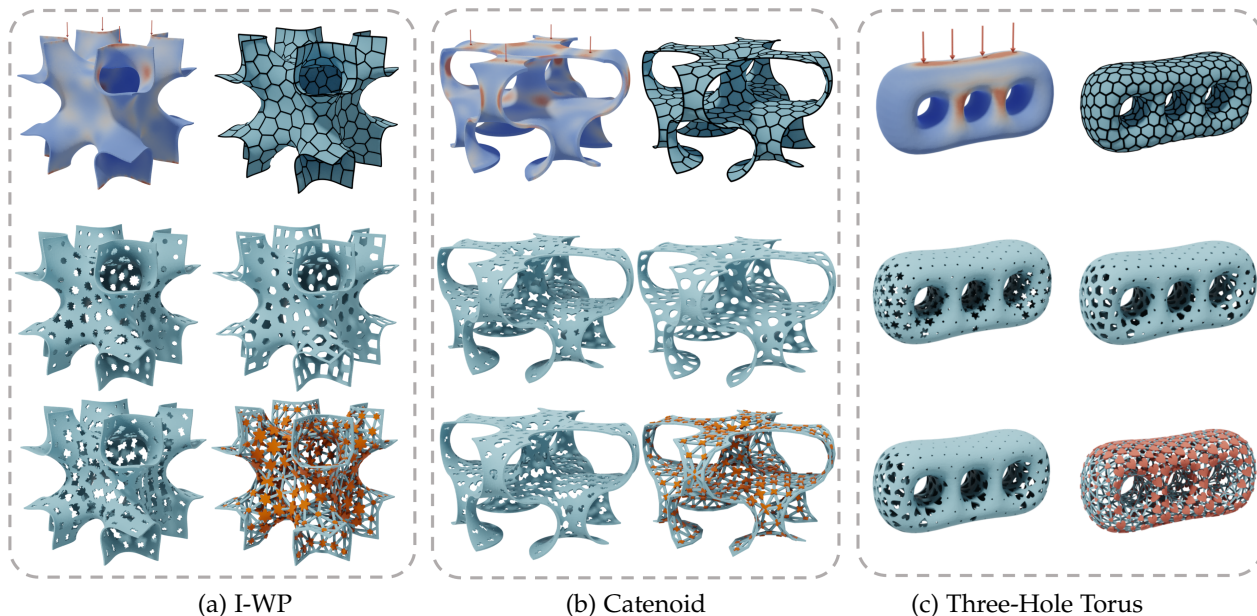(a) I-WP   (b) Catenoid   (c) Three-Hole Torus

Fig. 10. More results with regular, irregular, customized, and dual patterns, respectively.

TABLE 1
Effectiveness and efficiency comparison between our method and commercial software (ANSYS). "♯ Parameters" means the number of optimized parameters, "♯ Elements" means the amount of background elements (the same resolution in ANSYS), e/e_0 is the compliance ratio of the engraved shell to the original model, "Time" is the time (minutes) to perform once physical analysis of an engraved shell structure, including meshing and analysis, "# Iterations" is the total number of iterations in our method.

Model	Pattern Type	# Parameters	# Elements	Volume (mm^3)		e/e_0		Time (min)		# Iterations
				Original Shell	Engraved Shell	Ours	ANSYS	Ours	ANSYS	
Building (Fig. 1)	Irregular	150	3,040,000	9.39	7.51	1.09	1.20	0.5	2.5	52
Panton Chair (Fig. 2)	Regular	300	2,703,584	8.98	6.72	1.04	1.20	0.8	3.1	60
I-WP (Fig. 10(a))	Regular	250	8,000,000	35.44	26.85	1.12	1.25	2.5	9.8	65
Catenoid (Fig. 10(b))	Customized (dual)	500	5,360,000	46.42	25.85	1.52	1.75	1.7	5.6	95
Three-Holes (Fig. 10(c))	Customized	800	1,329,160	17.22	13.22	1.06	1.18	1.9	6.2	115

(a) $e/e_0 = 1.43$ (b) $e/e_0 = 1.34$
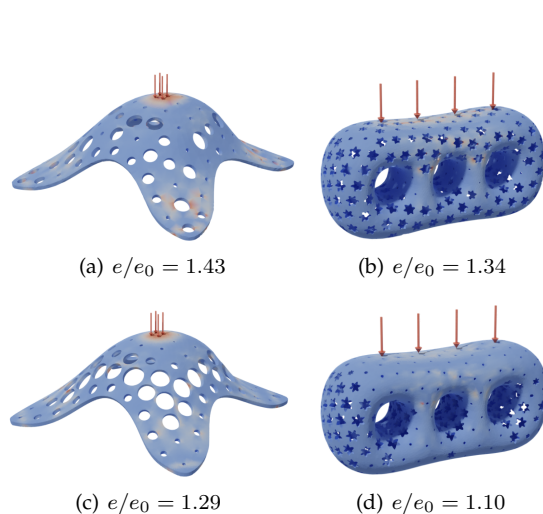
(c) $e/e_0 = 1.29$ (d) $e/e_0 = 1.10$

Fig. 11. Comparison between the discrete triangle element based method [11] (row 1) and our method (row 2). Our results have higher structural stiffness (smaller compliance ratio e/e_0) under the same volume constraints.
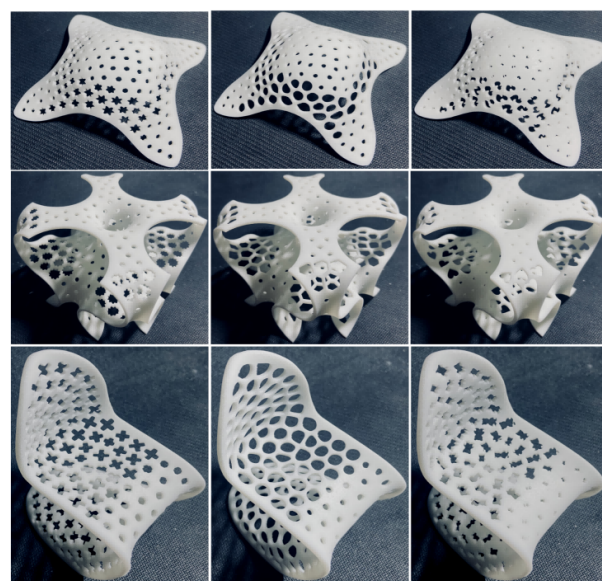

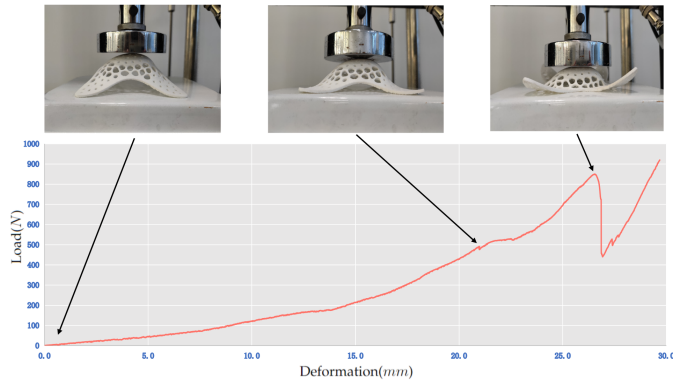Fig. 12. 3D printed shell models engraved by regular, irregular, and customized patterns, respectively.

Fig. 13. Stress testing of 3D printed models (maximum width 10cm; material: PLA; Young's modulus (GPa):0.03). Our structures can withstand a high external force (over 500 N), and the supporting legs do not break until the testing machine applies force over 800 N.

practicality, we also test a 3D printed model using an RG1-5 microcomputer control electronic universal testing machine, as shown in Fig. 13. Our structure has a good mechanical performance. We observe that the structure can withstand a high external force, and the support legs do not break until the testing machine applies force over 800 N.
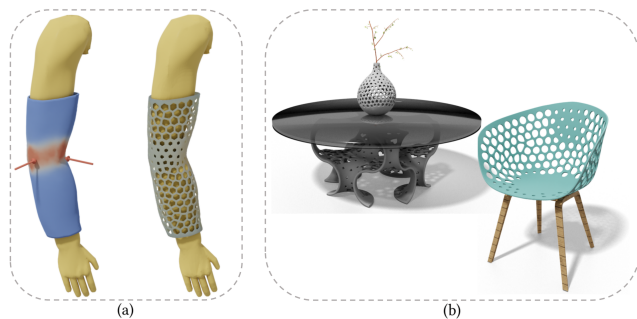

Fig. 14. Applications. (a) Lightweight medical gear. (b) Furniture design.

6.4 Applications

We apply our proposed algorithm to a variety of physically viable applications. For personalized medical gears, our engraving design can meet the requirements of lightweighting and heat dissipation while maintaining the necessary strength, as shown in Fig. 14 (a). We also illustrate the application in the field of living. Our method not only achieves the lightweight purpose but also dramatically enriches the diversity of furniture and household items, as shown in Fig. 14 (b).

6.5 Discussions

The proposed computational framework is in the form of implicit functions for representing, designing, and optimizing engraved structures. However, in our current implementation, we compute restricted centroidal Voronoi tessellation on triangular mesh surfaces to determine the positions of the patterns. It is worth noting that there are several techniques that can eliminate the requirement of triangular meshes. For

example, Leung et al. [57] proposed a unified framework for computing Voronoi tessellations on various types of 3D input, including implicit surfaces, polyhedral surfaces, and point clouds. Adopting this technique could make our method completely meshless.

7 CONCLUSIONS

We proposed a new parametric design and optimization for physically viable thin-shells. Since our method represents both the shell and patterns by implicit functions, it enables (dual) engraving of regular, irregular, and customized patterns as function operations. We formulate the design problem by optimizing the sizes and orientations properties of patterns and evaluating the parameters to minimize the strain energy of structures under a specified volume constraint. Since the engraved structures are represented by implicit functions, our method can avoid remeshing during optimization iterations. Through simulation and 3D printing, we show that the proposed method is more effective than methods based on traditional FEM and enriches the diversity of shell structure design.

Our approach calls for possible further improvements that will be addressed in follow-up research. First, we consider only thin shells with constant thickness in our current implementation. It is desired to take thickness as a variable in the optimization. Second, we assume the patterns are flat in this paper. Our method can be extended to curved patterns. A possible way is to utilize the Local Barycentric Coordinates technique [58], and we can bend patterns according to shell curvature by adjusting control grids (like the control grids shown in Fig. 4(c)). Third, we would like to investigate support-free pattern engraving in future work to make our method of 3D printing friendly.

ACKNOWLEDGMENTS

REFERENCES

[1] S. Adriaenssens, P. Block, D. Veenendaal, and C. Williams, *Shell structures for architecture: form finding and optimization*. Routledge, 2014.

[2] M. Melaragno, *An introduction to shell structures: The art and science of vaulting*. Springer Science & Business Media, 2012.

[3] N. Pietroni, D. Tonelli, E. Puppo, M. Froli, R. Scopigno, and P. Cignoni, "Statics Aware Grid Shells," *Computer Graphics Forum*, vol. 34, no. 2, pp. 627–641, 2015.

[4] W. Chen, X. Zhang, S. Xin, Y. Xia, S. Lefebvre, and W. Wang, "Synthesis of filigrees for digital fabrication," *ACM Transactions on Graphics*, vol. 35, no. 4, pp. 1–13, 2016.

[5] X. Liu, L. Lu, A. Sharf, X. Yan, D. Lischinski, and C. Tu, "Fabricable dihedral escher tessellations," *Computer-Aided Design*, vol. 127, pp. 1–10, 2020.

[6] J. Yang, S. He, and L. Lin, "Binary Image Carving for 3D Printing," *Computer-Aided Design*, vol. 114, pp. 191–201, 2019.

[7] P. Stadlbauer, D. Mlakar, H.-P. Seidel, M. Steinberger, and R. Zayer, "Interactive Modeling of Cellular Structures on Surfaces with Application to Additive Manufacturing," *Computer Graphics Forum*, vol. 39, no. 2, pp. 277–289, 2020.

[8] X. Zhang, G. Fang, C. Dai, J. Verlinden, J. Wu, E. Whiting, and C. C. Wang, "Thermal-Comfort Design of Personalized Casts," in *Proceedings of the 30th Annual ACM Symposium on User Interface Software and Technology*. ACM, 2017, pp. 243–254.

[9] C. Rao, L. Tian, D.-M. Yan, S. Liao, O. Deussen, and L. Lu, "Consistently fitting orthopedic casts," *Computer Aided Geometric Design*, vol. 71, pp. 130–141, 2019.

[10] J. Dumas, A. Lu, S. Lefebvre, J. Wu, and C. Dick, "By-example synthesis of structurally sound patterns," *ACM Transactions on Graphics*, vol. 34, no. 4, pp. 1–12, 2015.

[11] C. Schumacher, B. Thomaszewski, and M. Gross, "Stenciling: Designing structurally-sound surfaces with decorative patterns," *Computer Graphics Forum*, vol. 35, no. 5, pp. 101–110, 2016.

[12] M. Bucalem and K.-J. Bathe, "Finite element analysis of shell structures," *Archives of Computational Methods in Engineering*, vol. 4, no. 1, pp. 3–61, 1997.

[13] F. Cirak, M. J. Scott, E. K. Antonsson, M. Ortiz, and P. Schröder, "Integrated modeling, finite-element analysis, and engineering design for thin-shell structures using subdivision," *Computer-Aided Design*, vol. 34, no. 2, pp. 137–148, 2002.

[14] J. Panetta, M. Konaković-Luković, F. Isvoranu, E. Bouleau, and M. Pauly, "X-shells: A new class of deployable beam structures," *ACM Transactions on Graphics*, vol. 38, no. 4, pp. 1–15, 2019.

[15] A. H. Bermano, T. Funkhouser, and S. Rusinkiewicz, "State of the art in methods and representations for fabrication-aware design," *Computer Graphics Forum*, vol. 36, no. 2, pp. 509–535, 2017.

[16] B. Bickel, P. Cignoni, L. Malomo, and N. Pietroni, "State of the art on stylized fabrication," *Computer Graphics Forum*, vol. 37, no. 6, pp. 325–342, 2018.

[17] M. Farshad, *Design and analysis of shell structures*. Springer Science & Business Media, 2013, vol. 16.

[18] M. Jawad, *Theory and design of plate and shell structures*. Springer Science & Business Media, 2012.

[19] J. Martínez, M. Skouras, C. Schumacher, S. Hornus, S. Lefebvre, and B. Thomaszewski, "Star-shaped metrics for mechanical metamaterial design," *ACM Transactions on Graphics*, vol. 38, no. 4, pp. 1–13, 2019.

[20] C. Schumacher, S. Marschner, M. Gross, and B. Thomaszewski, "Mechanical characterization of structured sheet materials," *ACM Transactions on Graphics*, vol. 37, no. 4, pp. 1–15, 2018.

[21] G. Turk, "Texture synthesis on surfaces," in *Proceedings of the 28th Annual Conference on Computer Graphics and Interactive Techniques*, ser. SIGGRAPH '01, 2001, p. 347–354.

[22] J. Zehnder, S. Coros, and B. Thomaszewski, "Designing structurally-sound ornamental curve networks," *ACM Transactions on Graphics*, vol. 35, no. 4, pp. 1–10, 2016.

[23] T. N. H. Le, S.-Y. Yao, C.-K. Yeh, S-J. Wang, and T.-Y. Lee, "Optimized binarization for eggshell carving art," in *SIGGRAPH Asia 2021 Posters*, 2021, pp. 1–2.

[24] A. N. Ahsan and B. Khoda, "Honeycomb pattern on thin wall object with grain based 3d printing," *Procedia Manufacturing*, vol. 26, pp. 900–911, 2018.

[25] C. Jiang, J. Wang, J. Wallner, and H. Pottmann, "Freeform honeycomb structures," *Computer Graphics Forum*, vol. 33, no. 5, pp. 185–194, 2014.

[26] C.-H. Peng, H. Pottmann, and P. Wonka, "Designing patterns using triangle-quad hybrid meshes," *ACM Transactions on Graphics*, vol. 37, no. 4, pp. 1–14, 2018.

[27] J. Liu, A. T. Gaynor, S. Chen, Z. Kang, K. Suresh, A. Takezawa, L. Li, J. Kato, J. Tang, C. C. Wang *et al.*, "Current and future trends in topology optimization for additive manufacturing," *Structural and Multidisciplinary Optimization*, vol. 57, no. 6, pp. 2457–2483, 2018.

[28] G. Allaire, E. Bonnetier, G. Francfort, and F. Jouve, "Shape optimization by the homogenization method," *Numerische Mathematik*, vol. 76, no. 1, pp. 27–68, 1997.

[29] M. P. Bendsøe, "Optimal shape design as a material distribution problem," *Structural optimization*, vol. 1, no. 4, pp. 193–202, 1989.

[30] M. Y. Wang, X. Wang, and D. Guo, "A level set method for structural topology optimization," *Computer Methods in Applied Mechanics and Engineering*, vol. 192, no. 1-2, pp. 227–246, 2003.

[31] Y. Xie and G. Steven, "A simple evolutionary procedure for structural optimization," vol. 49, pp. 885–896, 1993.

[32] W. Zhang, J. Yuan, J. Zhang, and X. Guo, "A new topology optimization approach based on moving morphable components (mmc) and the ersatz material model," *Struct Multidisc Optim*, vol. 53, pp. 1243–1260, 2016.

[33] L. Cheng, J. Bai, and A. C. To, "Functionally graded lattice structure topology optimization for the design of additive manufactured components with stress constraints," *Computer Methods in Applied Mechanics and Engineering*, vol. 344, pp. 334–359, 2019.

[34] J. Hu, S. Wang, B. Li, F. Li, Z. Luo, and L. Liu, "Efficient representation and optimization for tpms-based porous structures," *IEEE Transactions on Visualization and Computer Graphics*, pp. 1–1, 2020.

[35] W. Wang, T. Wang, Z. Yang, L. Liu, and X. Liu, "Cost-effective printing of 3d objects with skin-frame structures," *ACM Transactions on Graphics*, vol. 32, no. 6, pp. 177:1–177:10, 2013.

[36] X. Zhang, Y. Xia, J. Wang, Z. Yang, C. Tu, and W. Wang, "Medial axis tree - an internal supporting structure for 3d printing," *Computer Aided Geometric Design*, vol. 35-36, pp. 149–162, 2015.

[37] S. Chai, B. Chen, M. Ji, Z. Yang, M. Lau, X.-M. Fu, and L. Liu, "Stress-oriented structural optimization for frame structures," *Graphical Models*, vol. 97, pp. 80–88, 2018.

[38] L. Lu, A. Sharf, H. Zhao, Y. Wei, Q. Fan, X. Chen, Y. Savoye, C. Tu, D. Cohen-Or, and B. Chen, "Build-to-last: Strength to weight 3d printed objects," *ACM Transactions on Graphics*, vol. 33, no. 4, pp. 97:1–97:10, 2014.

[39] T. Kuipers, J. Wu, and C. C. Wang, "CrossFill: Foam Structures with Graded Density for Continuous Material Extrusion," *Computer Aided Design*, vol. 114, pp. 37–50, 2019.

[40] W. Wang, Y.-J. Liu, J. Wu, S. Tian, C. C. Wang, L. Liu, and X. Liu, "Support-free hollowing," *IEEE Transactions on Visualization and Computer Graphics*, vol. 24, no. 10, pp. 2787–2798, 2017.

[41] S. J. Hollister and N. Mater, "Porous scaffold design for tissue," *Natural Materials*, vol. 4, pp. 518–524, 2005.

[42] C. Schroeder, W. C. Regli, A. Shokoufandeh, and W. Sun, "Computer-aided design of porous artifacts," *Computer Aided Design*, vol. 37, pp. 339–353, 2005.

[43] C. Schumacher, J. Zehnder, and M. Bächer, "Set-in-stone: worst-case optimization of structures weak in tension," *ACM Transactions on Graphics*, vol. 37, no. 6, pp. 252:1–252:13, 2018.

[44] R. Prevost, E. Whiting, S. Lefebvre, and O. Sorkine-Hornung, "Make it stand: Balancing shapes for 3d fabrication," *ACM Transactions on Graphics*, vol. 32, no. 4, pp. 81:1–81:10, 2013.

[45] M. Skouras, B. Thomaszewski, S. Coros, B. Bickel, and M. Gross, "Computational design of actuated deformable characters," *ACM Transactions on Graphics*, vol. 32, no. 4, pp. 82:1–82:10, 2013.

[46] M. Bacher, E. Whiting, B. Bickel, and O. Sorkine-Hornung, "Spin-it:optimizing moment of inertia for spinnable objects," *ACM Transactions on Graphics*, vol. 33, no. 4, pp. 96:1–96:10, 2014.

[47] J. Wu, N. Aage, R. Westermann, and O. Sigmund, "Infill optimization for additive manufacturing – approaching bone-like porous structures," *IEEE Transactions on Visualization and Computer Graphics*, vol. 24, no. 2, pp. 1127–1140, 2018.

[48] J. Martínez, J. Dumas, S. Lefebvre, and L.-Y. Wei, "Structure and appearance optimization for controllable shape design," *ACM Transactions on Graphics*, vol. 34, no. 6, pp. 1–11, 2015.

[49] E. Cohen, R. F. Riesenfeld, and G. Elber, *Geometric modeling with splines: an introduction*. CRC Press, 2001.

[50] S. Skyum, "A simple algorithm for computing the smallest enclosing circle," *Information Processing Letters*, vol. 37, no. 3, pp. 121–125, 1991.

[51] B. Lévy and Y. Liu, "L p centroidal voronoi tessellation and its applications," *ACM Transactions on Graphics (TOG)*, vol. 29, no. 4, pp. 1–11, 2010.

[52] A. Vaxman *et al.*, "Directional: A library for Directional Field Synthesis, Design, and Processing," 2021. [Online]. Available: https://doi.org/10.5281/zenodo.3338174

[53] T. H. Nguyen, G. H. Paulino, J. Song, and C. H. Le, "A computational paradigm for multiresolution topology optimization (MTOP)," *Structural and Multidisciplinary Optimization*, vol. 41, no. 4, pp. 525–539, 2010.

[54] C. Liu, Y. Zhu, Z. Sun, D. li, Z. Du, W. Zhang, and X. Guo, "An efficient moving morphable component (mmc)-based approach for multi-resolution topology optimization," *Structural and Multidisciplinary Optimization*, vol. 58, no. 6, pp. 2455–2479, 2018.

[55] K. Svanberg, "A class of globally convergent optimization methods based on conservative convex separable approximations," *SIAM Journal on Optimization*, vol. 12, no. 2, pp. 555–573, 2002.

[56] Z.-Y. Wu, F. Bai, and L.-S. Zhang, "Convexification and concavification for a general class of global optimization problems," *Journal of Global Optimization*, vol. 31, no. 1, pp. 45–60, 2005.

[57] Y.-S. Leung, X. Wang, Y. He, Y.-J. Liu, and C. C. Wang, "A unified framework for isotropic meshing based on narrow-band euclidean